Microstructure of polyacrylate/polystyrene two-stage latices

M. S. Silverstein, Y. Talmon and M. Narkis*

Department of Chemical Engineering, Technion–Israel Institute of Technology, Haifa 32000, Israel

(Received 8 June 1988; accepted 14 July 1988)

The microstructure of multi-stage latices is investigated in the cold stage of the transmission electron microscope (TEM) through differences in the behaviour of their component polymers when irradiated by an electron beam. Frozen two-stage latices (TSL) of polyacrylates (PA) and polystyrene (PS) are examined in the TEM and in a high resolution scanning electron microscope (SEM). A PS core is revealed in a frozen PS seeded PS/PA TSL in the TEM. Crosslinked PS (XPS) shells are observed in the TEM of a frozen crosslinked PA (XPA) seeded XPA/XPS TSL with 50% PS. The identity of the particles with XPS shells is retained in the moulded material and observed in SEM. The existence of an interpenetrating polymer network (IPN)/microdomain structure is indirectly indicated in XPA seeded XPA/XPS TSL with 25% XPS whose mechanical behaviour also favours an XPA continuum and both intra- and inter-particle XPS microdomains. IPN/microdomain particles and particles with XPS shells in an XPA seeded XPA/XPS TSL with 35% XPS are observed in the TEM and reflected in the structure of the moulded material.

(Keywords: latices; polyacrylates; polystyrene; structure)

INTRODUCTION

Multiphase polymeric materials exhibit properties that are often superior to those of their component homopolymers due to the unique morphological structure and the existence of phase separated domains[1,2]. These phase separated domains can be rigid, reinforcing an elastomer (styrene–butadiene–styrene triblock copolymers), or rubbery, increasing the impact resistance of a plastic (acrylonitrile–butadiene–styrene, ABS). The contrast needed for transmission electron microscopy (TEM) studies of these multiphase polymeric materials has been attained by fixation and staining of the unsaturated rubbery phase with osmium tetroxide[3]. Multiphase polymers that do not contain an unsaturated phase are not easily stained. In order to characterize their morphology by electron microscopy more complex sample preparation techniques must be used[4–8].

Frozen polymer latices have been used as a model system in the study of the electron beam radiation damage to organic inclusions in ice[9–11]. In an ice matrix radiolysed polystyrene (PS) undergoes mainly crosslinking while radiolysed polyacrylates (PA) and polymethacrylates undergo mainly scission[12,13]. This difference in behaviour can be used to distinguish between PS and PA particles. A variety of two-stage latices (TSL) of PA and PS examined in the TEM have revealed morphologies that correspond to those deduced from mechanical and rheological analyses[12–14].

Interpenetrating polymer networks (IPN) materials, ideally consisting of two homopolymer networks interwoven on a molecular level, are often, in practice, classified as multiphase polymeric materials[15]. Bulk IPN are synthesized by either the simultaneous polymerization and crosslinking of two monomers through mutually exclusive mechanisms or the polymerization and crosslinking of monomer II swelling a crosslinked polymer I. These materials may have a multiphase morphology due to the partial or complete incompatibility of the component polymers that leads to their subsequent phase separation. The enhanced mixing of incompatible polymers in IPN is due to a hindering effect imposed on the phase separation process by the constraints of the interlocking network structure of the crosslinked polymers[16–19]. The phase separation of polymer II in sequential bulk IPN may affect the material's bicontinuous nature and could, in the extreme case, limit polymer continuity. An IPN-like polymerization with only one of the polymers crosslinked yields a semi-IPN, a semi-1-IPN with only polymer I crosslinked, and a semi-2-IPN with only polymer II crosslinked.

The combination of elastomeric and rigid polymers in an IPN can yield a variety of materials whose properties vary from a reinforced elastomer to a high impact plastic. The composition, size, distribution and continuity of the IPN components synthesized from different materials have been characterized through dynamic mechanical spectroscopy (d.m.s.), differential scanning calorimetry (d.s.c.) and electron microscopy[20–24]. The importance of the composition and degrees of crosslinking in bulk IPN has been revealed through their influence on both the domain size in SEM micrographs and the mechanical properties of the material[25]. The major limitation of these bulk IPNs is that they are not processable because of their thermosetting nature.

The synthesis of latex IPN (LIPN) materials using a two-stage latex (TSL) emulsion polymerization (the polymerization of monomer II and crosslinker on a crosslinked polymer I seed latex) may yield materials of significant mechanical properties that can be processed using standard thermoplastic methods and machinery[14,26,27]. Elastomeric LIPN particles of crosslinked PS on a crosslinked PA seed, have been

* To whom correspondence should be addressed

0032-3861/89/030416-09$03.00

characterized as having intraparticle PS microdomains, based on mechanical, rheological, thermal and TEM studies. Two levels of structure in such moulded LIPN, inside the particles and between the particles, must be taken into account not only for their contribution to the significant modulus and tensile strength, but also for their effect upon the flow properties of the LIPN. Direct evidence of the existence of these microdomains, however, is still lacking. An investigation of LIPN morphology is reported in this paper through the examination of moulded TSL materials of various compositions and degrees of seed crosslinking using TEM and high resolution scanning electron microscopy (SEM).

EXPERIMENTAL

Emulsion polymerization

Standard emulsion polymerization procedures[28–30] were used in both stages of the semi-batch synthesis of the sequential two-stage latex, where both the organic and aqueous components were added continuously. The TSL in this study result from the sequential polymerization of styrene to which 0.25 mass per cent divinyl benzene (DVB) has been added as a crosslinking agent, on a crosslinked PA seed latex (the acrylate is 70% butyl acrylate and 30% ethyl acrylate to which butadiene, BD, has been added as the crosslinking agent). Two series of TSL were examined. The first had a constant polymer composition (PA/PS 75/25) and varying degrees of PA seed crosslinking (0, 1.5, 3 and 4.5 mass per cent BD). The second series had a constant degree of crosslinking in the PA seed (3% BD) and varying compositions (25%, 35%, 50% and 75% PS; there was no DVB in the 75% PS sample). Each stage in the polymerization recipe had an aqueous to organic ratio of 2:1. The TSL were coagulated through the addition of methanol. The crumb was dried overnight at 60°C in an vacuum oven, and then compression moulded at 20 MPa, 180°C.

Cold-stage transmission electron microscopy

Thin frozen specimens for the cold-stage TEM procedure[9,10,12,13] were prepared using the double-film technique in which a layer of diluted latex, less than 0.5 μm thick, was sandwiched between two polyimide film covered grids and frozen in liquid nitrogen. The frozen latex samples were examined with 100 kV electron beam at 95 K by finding a suitable area at low magnification, and recording a series of micrographs at 20000× until approximately 5 min had elapsed, corresponding to electron exposures (doses) of 2–150 kC/m^2.

Scanning electron microscopy

Specimens were prepared for the SEM by fracturing the moulded LIPN material under liquid nitrogen. The fractured pieces were trimmed to a height of about 4 mm and mounted on SEM stubs using colloidal graphite cement. The specimens were sputter-coated with a thin layer (approximately 20 nm) of gold in a Hexaland CT100 Cryotrans system attached to the SEM. Then, without exposure to the ambient atmosphere, the specimens were transferred into the SEM, a Hitachi S-800 microscope equipped with a field-emission gun. This electron source produces a very bright and fine electron beam, providing excellent signal-to-noise ratio and high resolution, not normally attainable in conventional SEM.

RESULTS AND DISCUSSION

The sequential emulsion polymerization procedure can yield a wide range of TSL morphologies dependent upon the sequence of polymerization, the composition, the relative hydrophilicity of the polymers, the mobility of the polymer (related to the glass transition and molecular weight), the solubility of polymer I in monomer II, the degree of crosslinking, the degree of grafting and the reaction conditions[31–43]. TSL morphologies that have been investigated in the past have yielded the following conclusions:

1. When polymer II is miscible with and more hydrophilic than polymer I, a core-shell (C/S) structure is formed[43].
2. When polymer II is miscible with polymer I and there is no difference in hydrophilicity, polymer II-rich outer layers are formed[32].
3. When polymer I is insoluble in monomer II, polymer II layers form on the surface of polymer I and a C/S structure is formed[43].
4. When monomer II swells polymer I, but polymer II is immiscible with polymer I, phase separation takes place. When the polymers are not crosslinked, domains whose size depends on the relative hydrophilicity of the polymers and their mobilities are formed[41,42]. When only polymer I is crosslinked, a semi-1-IPN that may contain phase-separated microdomains is formed[44–46]. When only polymer II is crosslinked, a semi-2-IPN that may contain phase-separated microdomains and have a polymer II-rich shell is formed[44,45]. When both polymers are crosslinked, an IPN that may contain phase-separated microdomains is formed[44,45].
5. When monomer II swells polymer I, and polymer II is immiscible with polymer I, as in point 4, but at high concentrations of monomer II, a polymer II-rich shell is formed over the core particle described in point 4.

Minimal grafting and crosslinking in immiscible polymer pairs may in some cases result in an eventual separation of the two polymers into a dumbbell morphology[37,38].

TEM of a frozen latex, a mixture of poly(methyl methacrylate) and PS homopolymer latices, is used to demonstrate the distinction between the particles in *Figure 1*. When PS particles, which are the larger spheres in *Figure 1a*, are exposed to the electron beam, they retain their shape, and do not look different in *Figure 1b*. PMMA particles, which are the smaller spheres in *Figure 1a*, lose mass and swell when irradiated. This causes them to develop a cellular appearance shown in *Figure 1b*. A C/S morphology, illustrated schematically in *Figure 2a*, results when acrylates are polymerized on a PS seed latex. The accompanying micrograph shows a PA shell that swells, loses mass and develops a cellular appearance, exposing a PS core. The morphology of an LIPN particle, illustrated schematically in *Figure 2b*, can result at low (25%) polymer II (PS) concentrations from a reversal of the sequence, i.e. the polymerization of styrene and crosslinker on a crosslinked PA (XPA) seed latex. The accompanying micrograph shows an LIPN of 25% crosslinked PS (XPS) on an XPA seed. The LIPN particles behave like PMMA homopolymer when irradiated, although there is a decrease in swelling for a given electron dose.

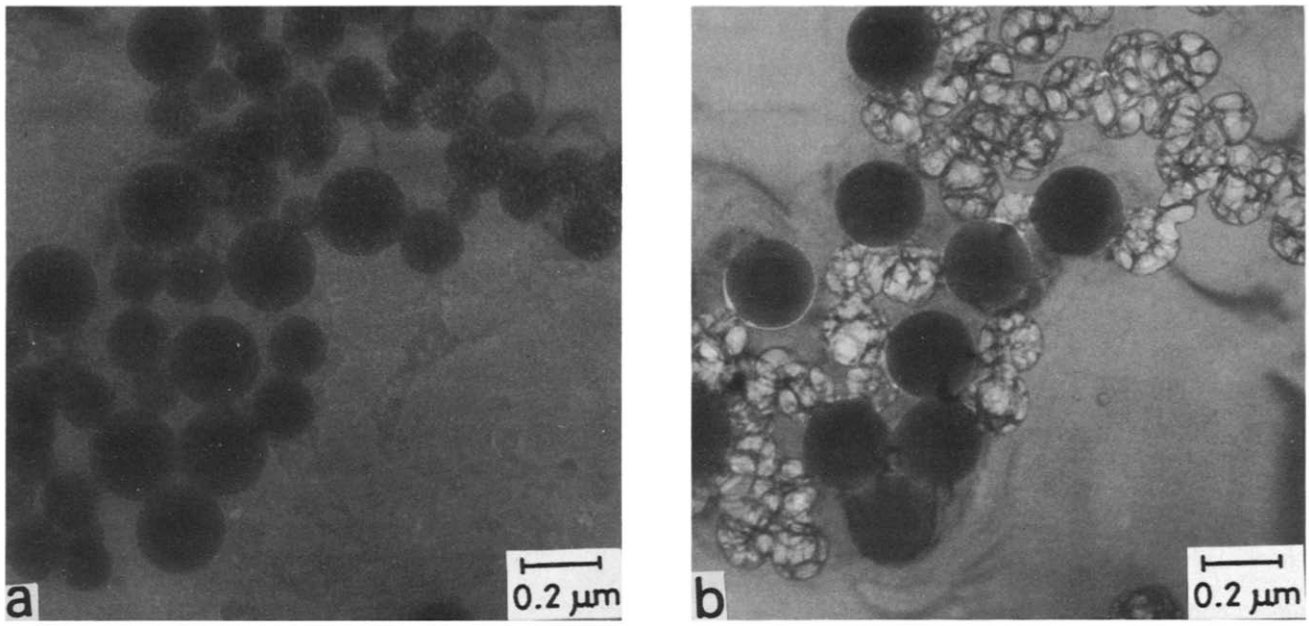

Figure 1 Irradiation of a frozen specimen of polymer latices in the TEM. Mixed latices: PMMA (smaller spheres) and PS (larger spheres). Electron exposure: (a) 2 kC/m^2; (b) 52 kC/m^2. After extensive irradiation the PMMA particles have a swollen and cellular appearance

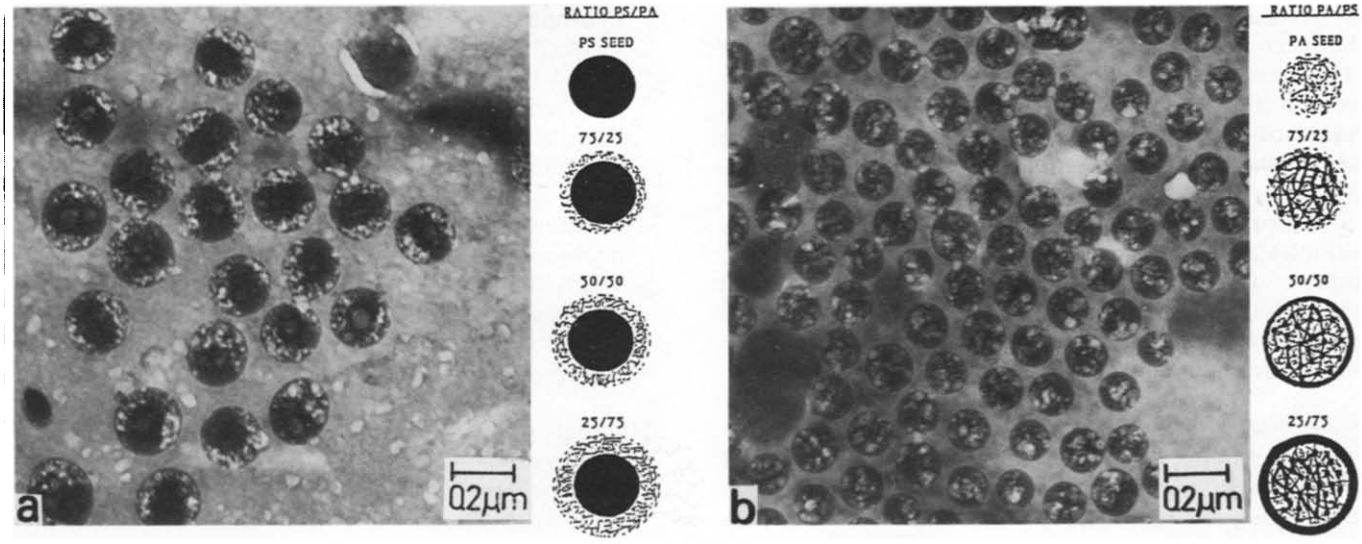

Figure 2 Irradiation of frozen two-stage latices in the TEM. (a) 25 PS/75 PA revealing a core/shell morphology. Schematic diagram shows variation of morphology with composition for a more hydrophobic, low mobility seed. Electron beam exposure: 80 kC/m^2. (b) 75 XPA/25 XPS has a radiation damage pattern similar to that of PMMA particles in *Figure 1*. No PS homopolymer particles, cores or shells are observed. Schematic diagram shows variation of morphology with composition for a more hydrophilic seed with both polymers crosslinked where an XPS-rich shell is formed on the LIPN/microdomain particle at high XPS compositions. Electron beam exposure: 44 kC/m^2

These differences between the C/S and LIPN morphologies are also reflected by the tensile properties of the moulded materials. The poor properties of the moulded C/S particles reflect the structure of the moulded material with the PA shells forming a continuous matrix containing embedded PS cores which act as a glassy filler[14,27]. The significant tensile strength of the moulded LIPN particles reflects the existence of PS inter-particle ties in a continuous XPA matrix whose strength increases with the PS concentration. The effect of the sequence of polymerization and the composition upon the morphology as revealed in the micrographs can also be reflected in the mechanical, thermal and rheological properties of the materials[44,45].

The absence of discrete PS homopolymer particles, cores or shells in *Figure 2b*, a 75 XPA/25 XPS TSL, indicates that there exist no PS domains larger than 50 nm in the TSL[12]. The T_g at approximately 100°C in the dynamic mechanical spectroscopy (d.m.s.) studies in *Figure 3* and in separate differential scanning calorimetry (d.s.c.) studies indicates the existence of a distinct PS phase that, to be detectable, must be at least on the order of 5 nm. The significant storage modulus revealed in this d.m.s. study indicates that the PS is not only of importance in the strength-forming mechanism connecting the particles, but also in their reinforcement through the formation of intra-particle PS microdomains. These considerations have led to the assumption that the morphology of these particles is that of an IPN combined with phase-separated PS microdomains.

The two levels of structure in a moulded 75 XPA/25

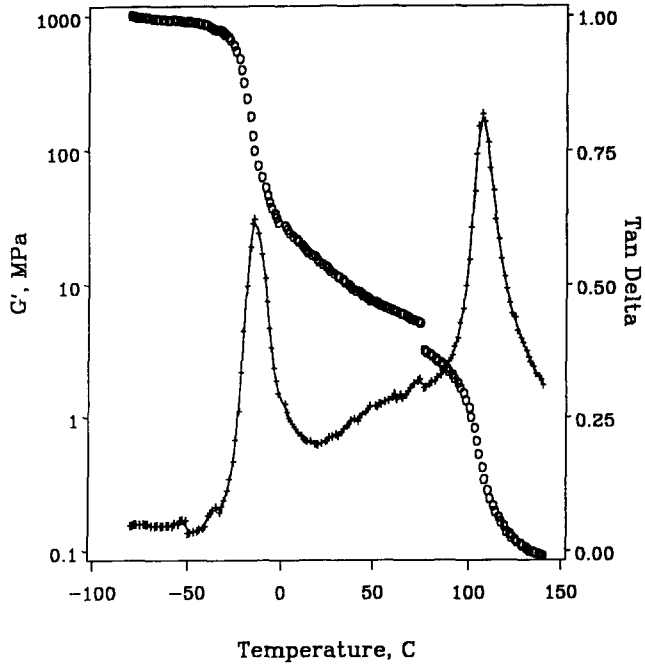

Figure 3 D.m.s. temperature sweep of moulded LIPN in torsion at 6 Hz. 75 XPA/25 XPS (PA: 85EA/15ethylhexylacrylate, 3% butadiene; PS crosslinked with 0.25% divinylbenzene). A significant storage modulus at room temperature and two glass transitions (one at −35°C and the other at 100°C) are observed. ○, G'; +, tan δ

XPS LIPN are illustrated schematically in *Figure 4*, where the presumed intra-particle morphology is a crosslinked PA seed, molecularly interwoven with, and perhaps grafted to a PS network containing grafted PS microdomains. The presumed inter-particle morphology is the mutual phase-separated PS microdomains connecting the moulded submicron particles. The intra-particle PS microdomains are responsible for the significant particle modulus, and the inter-particle domains are responsible for the significant tensile strength of the moulded material. Unlike unprocessable thermoset bulk IPN, the physical inter-particle ties soften and disintegrate at temperatures above the PS T_g and allow the processable LIPN to flow through a particle slip, stick and roll mechanism. The flow units are the submicron LIPN particles which have these interchangeable PS physical 'crosslinks', inter-particle microdomains. The submicron particles regain their shape upon the cessation of shear, and their behaviour when processed is, overall, similar to that of thermoplastics.

Increasing the amount of PS in this LIPN, as illustrated schematically in *Figure 2b*, leads, at a certain stage, to the formation of a PS-rich shell around the particle's IPN/microdomain structure. The formation of the PS shell may not occur simultaneously on all particles. Preferential polymerization may occur in PS-containing particles due to the greater affinity of styrene and the resulting larger surface area. This morphological transition, from LIPN to LIPN with PS shell, has an important effect on the moulded materials, because the former has continuous XPA, or apparently a bicontinuous structure (depending on the extent of phase separation), whereas in the latter the XPA continuity diminishes and may even disappear at higher PS concentrations. Thus the LIPN particles are completely surrounded by XPS-rich shells at 50% XPS on a XPA seed. When irradiated, the particles with PS shells in *Figure 5a* behave like the PS homopolymer in *Figure 1*, because the XPA is contained within the XPS shell[12,13]. Discrete particles of 100 to 120 nm are seen in the high resolution SEM micrograph of a fracture surface of this TSL in *Figure 5b*. The flow mechanism of the lightly crosslinked LIPN particles with lightly crosslinked PS shells at elevated temperatures has the deformable latex particles as flow units that regain their shape upon the cessation of shear. The inter-particle ties in these crosslinked 50:50 systems formed under hindered coalescence conditions during the flow moulding operation are weaker than the XPS shells and, as a result, the fracturing process propagates along the weak particle–particle contours. Thus, the crosslinked PS shells retain their general identity after moulding and their surface is exposed by low temperature fracturing as seen in *Figure 5b*.

The beginning of the formation of XPS-rich shells on some of the LIPN particles at 35% XPS can be seen in *Figure 5c*, where two particle populations of similar size exist whose behaviour, when irradiated, is different. The particles with the LIPN morphology lose mass, swell and become cellular in appearance, like the PMMA particles in *Figure 1*, while the LIPN particles with XPS-rich shells behave like the PS particles in *Figure 1*. The fracture surface of this TSL with 35% XPS on an XPA seed, that has both LIPN particles and LIPN particles with an XPS shell, reveals in *Figure 5d* a surface that contains both a particle structure, as seen in *Figure 5b*, and a structure that reflects the LIPN particles.

The XPS in an LIPN, contained within the particle as microdomains, estimated to be between 5 and 40 nm, and as an interwoven network structure, cannot be directly observed in *Figure 6a*, where the particles undergo mass loss and swelling similar to PMMA. The fracture surface of a moulded LIPN, 75 XPA/25 XPS with 1.5% BD in the seed, in *Figure 6b* does not exhibit the type of particle structure on the order of 100 nm observed in *Figure 5b*, in spite of the expectation that the particle structure in these crosslinked network materials is preserved. The structure observed in this micrograph, on the order of 20 nm in diameter, has been observed as well in the high resolution SEM for a homopolystyrene fracture surface, but not for

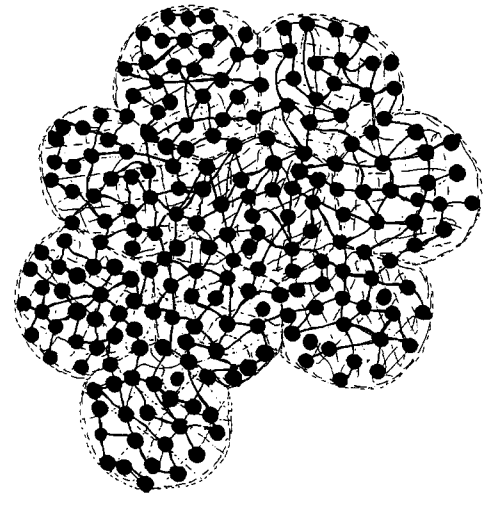

Figure 4 Schematic cross-section of moulded latex IPN showing intra-particle and inter-particle PS microdomains and an interwoven network structure. (●) PS microdomains; (——) PS network; (– – –) PA network

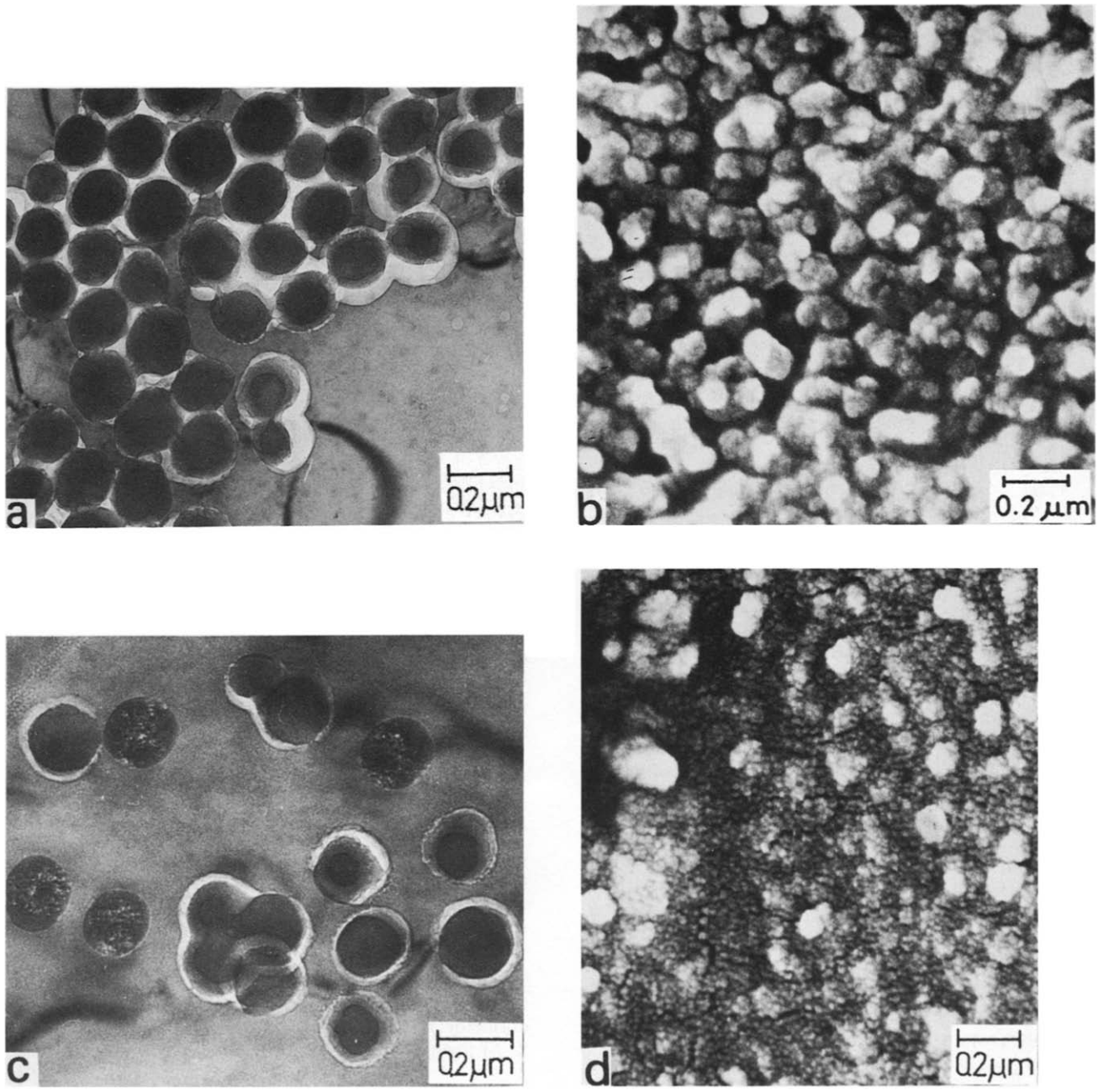

Figure 5 TSL particles and moulded sample structure with composition varied. (a) Frozen 50 XPA/50 XPS latex in TEM revealing particles with an XPS-rich shell. Electron beam exposure: 130 kC/m^2. (b) 50 XPA/50 XPS fracture surface in SEM revealing a structure of approximately 100 nm reflecting particles with XPS-rich shells in the moulded material. (c) Frozen 65 XPA/35 XPS latex in TEM revealing both LIPN particles, as in *Figure 2b*, and particles with an XPS-rich shell. Electron beam exposure: 69 kC/m^2. (d) 65 XPA/35 XPS fracture surface in SEM revealing in the moulded material both a structure of approximately 100 nm reflecting particles with XPS-rich shells and a structure reflecting the presence of the LIPN particles

an acrylate polymer fracture surface. The freeze fracture and ion beam sputtering process may both have contributed to the formation of this surface decoration artifact. A larger critical nucleus of sputtered metal is necessary in the coating of polystyrene due to its lower surface free energy, approximately one third of that of the more polar polyacrylates[47]. The uniform structure of the LIPN fracture surface in *Figure 6b* confirms the absence of XPS shells around the particle, which would yield the 100 nm particle structure seen in *Figure 5b*, and the presence of PS within the LIPN particles. Thus the surface decoration structure artifact in these materials might somehow reflect the nature of the underlying surface.

A TSL polymerized in the same manner as an LIPN but with the crosslinker left out of one of the stages may be referred to as a semi-LIPN, with a semi-2-LIPN indicating that there was no crosslinking in the first stage. The semi-2-LIPN of 75 PA/25 XPS has an unexpected PS-like storage modulus plateau that is significantly different than those of LIPN with various degrees of seed crosslinking[45]. The TEM analysis of this semi-2-LIPN in *Figure 6c* reveals a morphology unlike those of the LIPN of similar composition. The particles are surrounded by an XPS-rich shell, much like those observed in LIPN at higher PS concentrations. The phase separation in the semi-2-LIPN is not limited by an interwoven network structure and enhanced grafting of the XPS to the PA

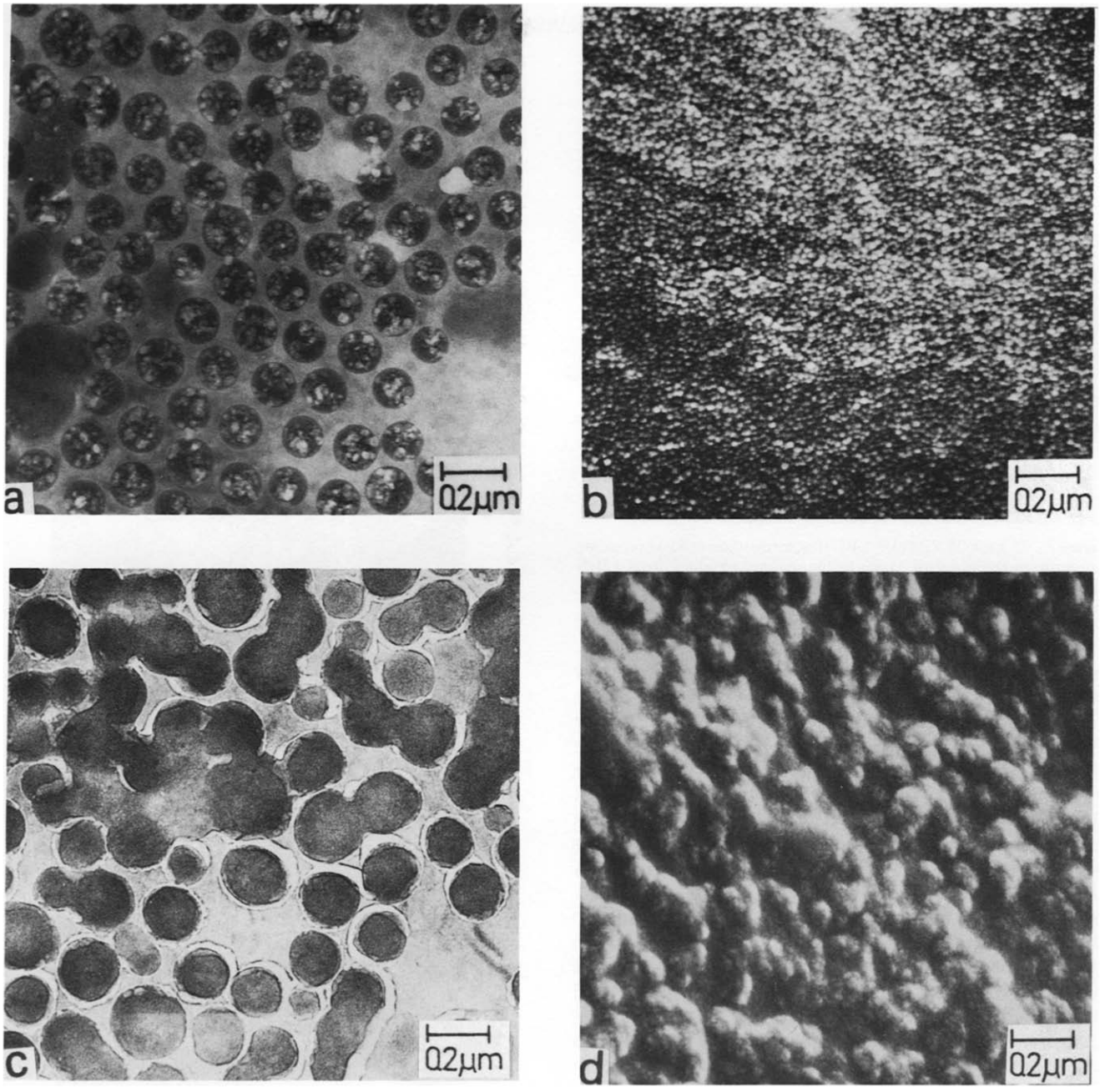

Figure 6 TSL particles and moulded sample structure with seed crosslinking varied. (a) Frozen 75 XPA/25 XPS latex in TEM revealing an LIPN morphology (as detailed in *Figure 2b*). Electron beam exposure: 44 kC/m^2. (b) 75 XPA/25 XPS (1.5% BD) fracture surface in SEM revealing structure on the order of 20 nm in the material moulded from LIPN particles. (c) Frozen 75 PA/25 XPS latex in TEM revealing particles with XPS-rich shells in the semi-2-LIPN. Electron beam exposure: 55 kC/m^2. (d) 75 PA/25 XPS fracture surface in SEM revealing a structure reflecting the particles with XPS-rich shells in the moulded semi-2-LIPN

through the residual unsaturation of the BD. This phase separation may result in the eventual formation of a dumbbell structure in the semi-2-LIPN particles[37,38]. The high resolution SEM micrograph of a moulded semi-2-LIPN in *Figure 6d* where the PA is a major component also exhibits a 100 nm particle structure somewhat similar to that observed in *Figure 5b* for particles with XPS-rich shells. Phase separation and formation of XPS-rich shells in the absence of PA crosslinking indicates the important role of the polymer I network in the LIPN morphology. Mixing of incompatible PA and PS is enhanced through the formation of an IPN structure. An increase in the PA crosslink density in the LIPN yields a decrease in the height of the PS tan δ peak in d.m.s. studies, presumably reflecting a decrease in the phase-separated PS microdomains[44,45]. The surface decoration observed in a fracture surface of an LIPN (75 XPA/25 XPS) with 3.0% BD in the seed in *Figure 7* yields a structure of approximately 15 nm, and that observed for an LIPN with 1.5% BD in the seed in *Figure 6b* yields a structure of approximately 20 nm.

A semi-1-LIPN results when the PA seed in the TSL is crosslinked but there is no crosslinker in the styrene in the second stage. Acrylonitrile–butadiene–styrene (ABS) is synthesized in this manner. Electron microscopy has revealed that at low styrene–acrylonitrile (SAN) concentrations the crosslinked rubbery polybutadiene latex particles contain SAN microdomains, with a

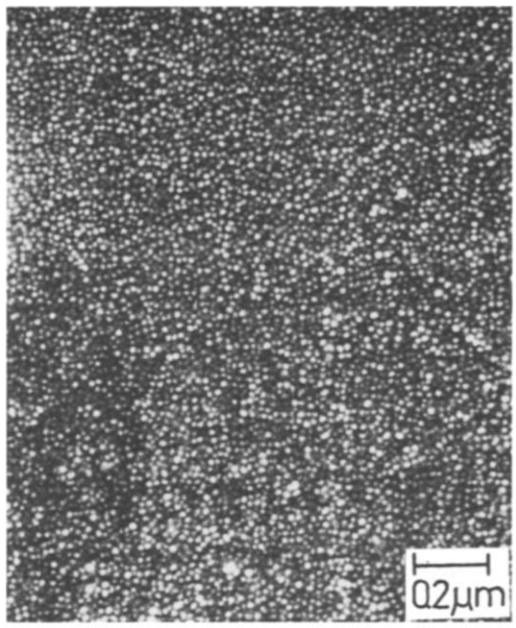

Figure 7 75 XPA/25 XPS (3.0% BD) fracture surface in SEM revealing structure on the order of 15 nm in the materal moulded from LIPN particles

profusion of domains on the particle's surface[46]. At higher SAN concentrations the SAN surface domains connect to form a shell. A TSL of 25 XPA/75 PS (PS not crosslinked) is such a semi-1-LIPN. The TEM analysis in *Figure 8a* reveals a bimodal particle distribution. The larger particles (300 nm) are XPA particles with a shell that behave much like the particles with XPS-rich shells under electron beam irradiation in *Figure 5a*. The smaller particles (60 nm) are XPA seed particles with no PS shells, and these undergo scission and mass loss. A polymerization mechanism that prefers to polymerize styrene in particles already containing PS may yield the two types of particles in *Figure 5c* with the LIPN particles with a PS shell the result of this preferential polymerization. The preferential polymerization mechanism would be more significant in 60 nm particles where less PS is needed to achieve the same effect seen in the 200 nm particles in *Figure 5c*. The smaller particle size may accelerate the phenomenon and yield the bimodal particle size distribution in *Figure 8a*.

The ripples on the fracture surface of this semi-1-LIPN in *Figure 8b* is somewhat similar to a surface typical of freeze fractured PS[48]. The structure of the original latex particles is not retained, as there is no crosslinker in the styrene to conserve the particle identity. Unlike the crosslinked PA seed, which does maintain its identity, the non-crosslinked PS shells flow when moulded and lose their identity by coalescing with neighbouring shells and forming a continuous thermoplastic PS matrix containing the dispersed submicron XPA particles. This continuous matrix structure of the major PS component is revealed in the rheological properties of the semi-1-LIPN that can flow through molecular deformation, as opposed to the particle slip-roll flow mechanism of the LIPN[44,45]. The 100 nm diameter indentations in the PS matrix seen in the SEM micrograph of a mould contact outer surface in *Figure 8c*, have a limited depth and correspond to the size of the holes shown in the fracture surface of *Figure 8b*. Mercury penetration under pressure and density studies have shown that the moulded samples are not porous, indicating that the cavities in *Figure 8b* were formed after the low temperature fracturing process and are not interconnected.

The fact that there are fewer indentations per unit area in the unfractured outer surface may be the result of a

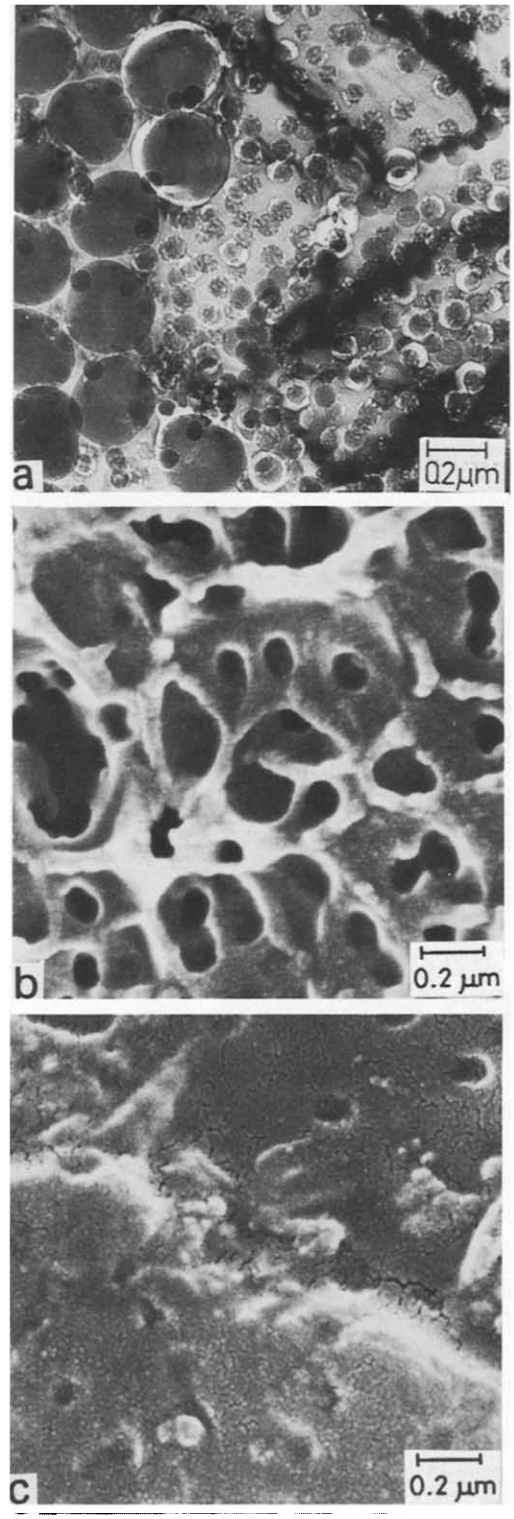

Figure 8 Structure of semi-1-LIPN, 25 XPA/75 PS. (a) Frozen latex in TEM revealing a bimodal particle size distribution consisting of TSL particles with PS shells (larger) and XPA seed particles (smaller). Electron beam exposure: 12 kC/m^2. (b) Fracture surface in SEM revealing structure somewhat similar to freeze fractured PS with holes on the order of 100 nm. (c) Mould contact surface in SEM revealing indentations on the order of 100 nm

difference between the outer skin and inner surface resulting from the moulding procedure. The origin of these holes is not obvious and is an important subject for future studies. The holes in this material may be the result of an artifact whose origins lie in the sample preparation procedures. These holes might also be related to the rubbery particles within the PS matrix. The fracture surface of ABS, where the rubbery particles have been removed by chemical etching with chromic acid, exhibit an almost identical morphology to that observed from *Figure 8b*[48,49].

CONCLUSIONS

The morphology of TSL particles from PA and PS can be elucidated by examination of their frozen latex in the TEM under the electron beam irradiation. A C/S particle morphology resulting from the polymerization of acrylates on a more hydrophobic PS seed in a PS/PA TSL is revealed in the TEM. The TEM of frozen latices also has revealed XPS shells in XPA seeded XPA/XPS TSL at 50% XPS. The identity of the original particles with XPS shells is retained in the moulded materials and a structure of approximately 100 nm, corresponding to that of the particles, is observed in the high resolution SEM. Shells of XPS are also revealed in TSL particles with 25% XPS when there is no crosslinking in the PA seed to limit the phase separation through the formation of an IPN structure.

There are no PS shells or individual PS homopolymer particles observed in the TEM of a frozen XPA seeded XPA/XPS TSL with 25% XPS. The behaviour of the moulded material indicates the existence of an IPN/microdomain structure. Although these particles are expected to retain their identity when moulded, no structure on the order of the 100 nm latex particles is revealed on the fracture surface of the moulded material in the SEM. The uniform structure of approximately 20 nm is presumably a surface decoration artifact from the sample preparation process that may reflect the nature and structure of the underlying surface. The XPA/XPS TSL with 35% XPS has both particles with an IPN/microdomain structure and particles with an XPS shell, and both types of structure are reflected in the fracture surface of the moulded material as observed by high resolution SEM.

A bimodal particle distribution consisting of 60 nm XPA particles and 300 nm particles with PS shells in an XPA seeded 25 XPA/75 PS TSL is revealed in the TEM examination of the frozen latex. This distribution may result from the preferential polymerization of styrene in latex particles with a higher PS concentration. The particles with PS shells, in contrast to those with XPS shells, are not expected to maintain their particle identity upon moulding. The holes of approximately 100 nm seen in the fracture surface of the moulded material in the SEM may have originated in the sample preparation details and presumably may be related to discrete XPA particles in the continuous thermoplastic PS matrix.

ACKNOWLEDGEMENT

The research of one of us (Y.T.) in cryo-electron microscopy has been supported by grants from the United States–Israel Binational Science Foundation (BSF), Jerusalem.

REFERENCES

1 Paul, D. R. and Newman, S. 'Polymer Blends', Academic Press, New York, 1978
2 Manson, J. A. and Sperling, L. H. in 'Polymer Blends and Composites', Plenum Press, New York, 1976
3 Kato, K. *Polym. Eng. Sci.* 1967, **7**, 38
4 Bucknall, C. B., Drinkwater, I. C. and Keast, W. E. *Polymer* 1972, **13**, 115
5 Sawyer, L. C. and Grubb, D. T. in 'Polymer Microscopy', Chapman and Hall, London, 1987
6 Hamazaki, T., Kanchiku, Y., Handa, R. and Izumi, M. *J. Appl. Polym. Sci.* 1977, **21**, 1569
7 Thomas, D. A. *J. Polym. Sci. Polym. Symp.* 1977, **60**, 189
8 White, J. R. and Thomas, E. L. *Rubber Chemistry and Technology* 1984, **57**, 457
9 Talmon, Y. *Ultramicroscopy* 1984, **14**, 305
10 Talmon, Y., Adrian, M. and Dubochet, J. *J. Microscopy* 1986, **141**, 375
11 Talmon, Y. in 'Cryotechniques in Biological Electron Microscopy' (Eds. R. A. Steinbrecht and K. Zierold), Springer-Verlag, Berlin, 1987, Ch. 3
12 Narkis, M., Talmon, Y. and Silverstein, M. S. *Polymer* 1985, **26**, 1359
13 Talmon, Y., Narkis, M. and Silverstein, M. S. *J. Elec. Micr. Technique* 1985, **2**, 589
14 Silverstein, M. S. and Narkis, M. *J. Appl. Polym. Sci.* 1987, **33**, 2529
15 Sperling, L. H. in 'Interpenetrating Polymer Networks and Related Materials', Plenum Press, New York, 1981
16 Sperling, L. H. *J. Polym. Sci. Macromolec. Rev.* 1977, **12**, 141
17 Klempner, D., *Angew. Chem. Int. Ed. Engl.* 1978, **17**, 97
18 Sperling, L. H. and Widmaier, J. M. *Polym. Eng. Sci.* 1983, **23**, 693
19 Yeo, J. K., Sperling, L. H. and Thomas, D. A. *Polym. Eng. Sci.* 1982, **22**, 190
20 Frisch, K. C., Klempner, D. and Frisch, H. L. *Polym. Eng. Sci.* 1982, **22**, 1143
21 Fox, R. B., Bitner, J. L., Hinkley, J. A. and Carter, W. *Polym. Eng. Sci.* 1985, **25**, 157
22 Hourston, D. J., Huson, M. G. and McCluskey, J. A. *J. Appl. Polym. Sci.* 1986, **31**, 709
23 Xiao, H. X., Frisch, K. C. and Frisch, H. L. *J. Polym. Sci., Polym. Chem. Edn.* 1983, **21**, 2547
24 Lee, J. H. and Kim, S. C. *Macromolecules* 1986, **19**, 644
25 Yeo, J. K., Sperling, L. H. and Thomas, D. A. *Polym. Eng. Sci.* 1981, **21**, 696
26 Silverstein, M. S. and Narkis, M. *Polym. Eng. Sci.* 1985, **25**, 257
27 Silverstein, M. S. and Narkis, M. *Polym. Plast. Technol. Eng.* 1987, **26**, 271
28 Bovey, F. A., Kolthoff, I. M., Medalia, A. I. and Meehan, E. J. in 'Emulsion Polymerization', Interscience, New York, 1955, Ch. IX
29 Gardon, J. L. *Rubber Chem. Technol.* 1970, **43**, 74
30 Vanderhoff, J. W. *J. Polym. Sci., Polym. Symp.* 1985, **72**, 161
31 Dickie, R. A. *J. Appl. Polym. Sci.* 1973, **17**, 45
32 Dickie, R. A., Cheung, M. F. and Newman, S. *J. Appl. Polym. Sci.* 1973, **17**, 65
33 Dickie, R. A. and Cheung, M. F. *J. Appl. Polym. Sci.* 1973, **17**, 79
34 Dimonie, V. L., El-Aasser, M. S., Klein, A. and Vanderhoff, J. W. *J. Polym. Sci., Polym. Chem. Edn.* 1984, **22**, 2197
35 Muroi, S., Hashimoto, H. and Hosoi, K. *J. Polym. Sci., Polym. Chem. Edn.* 1984, **22**, 1365
36 El-Aasser, M. S., Makgawinata, T. and Vanderhoff, J. W. *J. Polym. Sci., Polym. Chem. Edn.* 1983, **21**, 2363
37 Min, T. I., Klein, A., El-Aasser, M. S. and Vanderhoff, J. W. *J. Polym. Sci., Polym. Chem. Edn.* 1983, **21**, 2845
38 Okubo, M., Katsuta, Y. and Matsumoto, T. *J. Polym. Sci., Polym. Lett. Edn.* 1982, **20**, 45
39 Morgan, L. W. *J. Appl. Polym. Sci.* 1982, **27**, 2033
40 Winnik, M. A. *Polym. Eng. Sci.* 1984, **24**, 87
41 Okubo, M., Yamada, A. and Matsumoto, T. *J. Polym. Sci., Polym. Chem. Edn.* 1980, **16**, 3219
42 Okubo, M., Yamaguchi, S. and Matsumoto, T. *J. Appl. Polym. Sci.* 1986, **31**, 1075

43 Lee, D. I. and Ishikawa, T. *J. Polym. Sci., Polym. Chem. Edn.* 1983, **21**, 147
44 Silverstein, M. S. and Narkis, M. *J. Appl. Polym. Sci.* submitted
45 Silverstein, M. S. and Narkis, M. in 'Advances in Interpenetrating Polymer Networks' (Eds. D. Klempner and K. C. Frisch), Technomic
46 Kato, K. *Japan Plastics* 1968, **2**, 6
47 Neugebauer, C. A. in 'Handbook of Thin Film Technology' (Eds. L. I. Maissel and R. Glang), McGraw-Hill, New York, 1970, pp. 8–26
48 Engle, L., Klingele, H., Ehrenstein, G. W. and Schaper, H. in 'An Atlas of Polymer Damage', Wolfe, Berlin, 1981, pp. 109, 179
49 Bucknall, C. B. in 'Toughened Plastics', Applied Science, London, 1977, p. 336